Two-phase image analysis approach to compute the diameter of nanomaterials

Preprint · January 2021

CITATIONS
0

READS
42

4 authors:

Sumit Kaushik
Czech Technical University in Prague
12 PUBLICATIONS **6** CITATIONS
SEE PROFILE

Preeti Kaushik
J. Heyrovský Institute of Physical Chemistry
6 PUBLICATIONS **10** CITATIONS
SEE PROFILE

Jan Slovák
Masaryk University
100 PUBLICATIONS **2,434** CITATIONS
SEE PROFILE

Lenka Zajíčková
Masaryk University
180 PUBLICATIONS **2,131** CITATIONS
SEE PROFILE

Two-phase image analysis approach to compute the diameter of nanomaterials

Sumit Kaushik[1], Preeti Kaushik[2,3], Jan Slovák[1], Lenka Zajíčková[2,3]
[1]Department of Mathematics and Statistics, Masaryk University, Brno, Czech Republic
[2]RG Plasma Technologies, Central European Institute of Technology, Masaryk University, Brno, Czech Republic
[3]Department of Physical Electronics, Faculty of Science, Masaryk University,
Brno, Czech Republic

Abstract

Transmission and scanning electron microscopy techniques provide necessary image analysis for the structural analysis of micro and nanomaterials. Diameter evaluation is essential in investigating the properties of nanotubes and nanofibers. Intensity profile-based methods are inadequate due to inhomogeneity of statistics and deficits like non-uniform illumination, presence of other objects like a supporting carbon membrane, catalytic particles, and overlapping nanotubes. We present a two-phase image analysis approach which can separate sections of nanotubes/nanofibers from the background and consequently employ localized curve evolution to account for non-homogeneity caused by variation of intensities. The method has an edge over traditional thresholding global and local methods. For its demonstration, we considered carbon nanotubes and polymer nanofibers. The approach is efficient in overcoming the above issues and computing the diameter of tubular and fibrous nanomaterials. The objective analysis confirms the above mentioned claims.

Keywords: image analysis; electron microscopy; carbon nanotubes; polymer nanofibers; local curve evaluation

1. Introduction

1D nanostructured materials like nanotubes, nanofibers and nanowires are widely popular because of their unusually high surface to volume ratio. The properties of these high aspect ratio structured materials are highly dependent on different characteristics and parameters. Hence there is a need to quantitatively characterize nanomaterials that analyze the materials in a better way. Until the computer aided image processing came into existence, only a qualitative analysis of transmission electron microscopy (TEM) and scanning electron microscopy (SEM) images was performed. But with the new image processing techniques, a quantitative analysis of nanomaterials is possible.

Carbon nanotubes (CNTs), since been firstly discovered by Iijima in 1991, has drawn the most research interests because of their unique geometry, morphology and properties [1]. These cylindrical carbon molecules have unusual thermal, electrical and mechanical properties which are valuable for nanotechnology, electronic optics and other fields of material science and technology. CNT diameter plays an important role in various applications. Grace et al. studied the effect of wall number in CNT/Si heterojunction solar cells [2] and effect of diameter of CNTs on the gas sensing was observed by Arash et al. [3].

Another 1D nanomaterial like polymer nanofibers find use in biomedical applications like tissue engineering [4][5], drug delivery [6], cancer treatment [7] and bone regeneration [8]. Hence, quantitative analysis leading to an efficient measurement is necessary. Different tools are available for evaluating parameters, but human bias and error hinders their efficiency. Ziabari and Mottaghitalab used distance transform algorithm to evaluate the diameter of electrospun nanofibers and showed it to be accurate and faster as compared to the manual method [9]. Binary thresholding technique was used to measure the porosity of nanofibrous mat for application in scaffolds in tissue engineering [10].

The evolution of image analysis for nanomaterial processing has led to better characterization in terms of evaluating structural parameters. Image analysis methods proved useful in dealing with automization and enhancing accuracy. Different analytical techniques are used to characterize their structure and morphology. Electron microscopy (TEM/SEM) has emerged as a powerful tool for capturing spatial features and real-space visualization of nanomaterials [11][12]. Gommes et al. developed a technique to measure the diameters of multi-walled carbon nanotubes (MWCNTs) using intensity profile [13]. Ivasawki et al. [14] computed diameter using Otsu thresholding

and morphological operations. Based on these operations authors in [15] detected cracks in SEM micrographs for qualitative and quantitative analysis. The choice of segmentation algorithm depends upon the microscopic images to be processed. There is no universal criterion of choice but it depends upon the features to be extracted [16] [17]. For instance, for curvilinear structure like cytoskeleton are segmented in work [18] using the designed algorithm called individual fiber segmentation (IFS). Kim et al. [19] used entropy based masking method for segmentation. Recently, Groom et al. [20] designed an efficient hybridized mean local thresholding algorithm for nanoparticle extraction. Other works in similar directions are [21]-[22]. In all these works of image analysis, segmentation is a crucial step affecting [25]-[26] the final outcome. Some of the earlier image analysis works are based on choosing a global threshold value for an image. These methods depend upon the value of the threshold to be computed globally or locally. The global methods select one value for the image which works under the assumption of well-separated background/foreground. There are a number of disadvantages associated with them e.g. segmented regions are not connected, irregular boundaries and sensitivity to noise. A new class of method was introduced by Sethian and Osher [32] using level sets for segmentation. These methods can be categorized as edge-based and region-based. In edge-based methods, the convergence of evolution of curves is decided by the image gradients (edges). Edges being sensitive to noise makes method too sensitive. Further, in many applications, edges of the objects of interests are not sharp and even may not exist or not well defined. Another demerit is the requirement to place the initial curve near the object of interest. Another category is known as region-based methods. These methods showed improvement under noise, but initial placement condition persisted. In seminal work of Chan-Vese [33] based on Mumford-Shah formulation does not require edges for convergence of curve evolution. Inhomogeneity of local statistics was still an issue, in one such work Lankton et al. [34] introduced localization of global energy to overcome this downside. In our case, problem is the presence of artifacts, non-uniform background, overlapping objects and variation of diameters across the image.

This work outlines two phase image analysis approach for calculating diameter of two types of nanomaterials: carbon nanotubes and polymer nanofibers. In the first phase, regions comprising sections of nanotubes are extracted using adaptive thresholding and morphological operations. This step not only achieves the requirement of initial curve placement but also removes the unnecessary parts of the image. In the second phase, accuracy is achieved using localized contour

evolution and diameter is computed. We have shown that the approach is better than traditional thresholding methods and proper choice of the initial contour can decrease the number of iterations required.

2. Materials and methods

2.1. Preparation and imaging of experimental samples

Two types of nanostructures were used for diameter evaluation: carbon nanotubes and polymer nanofibers. Synthesis methods for these materials are described below.

CNTs were prepared on Si substrates coated with the 235 nm thick SiO_2 film using the procedure described previously [35]. The catalytic Fe film, 5 nm thick, was deposited by electron beam evaporator (BESTEC, Germany). The MWCNTs were grown in high temperature chemical vapor deposition (CVD) reactor by Oxford Instruments (Ar = 1000 sccm, H_2 = 200 sccm, C_2H_2 = 20 sccm). The process started by heating the table heater to 750 °C, followed by hydrogen stabilization for 1 min, pretreatment for 10 min in argon and hydrogen atmosphere and finally growth process for 20 min with C_2H_2 as a precursor. The pressure throughout was constant to 133 Pa. After cooling down the table heater to 695 °C the samples were taken out from the loadlock. The samples for high resolution transmission electron microscopy (HR-TEM) were prepared by dispersing the as grown MWCNTs on Si/SiO_2 substrates in demineralized water by the ultrasonic cleaner. The solution was put on a TEM grid with a carbon holey membranem and dried. This procedure resulted in well-separated CNTs on the grid without any presence of contamination. TEM characterization of MWCNTs was done using HR-TEM TITAN Themis 60-300 (Thermo Scientific, Netherlands) equipped with Cs-image corrector and monochromator. The TEM was operated at 60 kV to prevent the amorphization of carbon structures by the electron beam.

Nanofibers were prepared by electrospinning of polycaprolactone (PCL) solutions [36]. The PCL granulated polymer was dissolved in a mixture of acetic acid (2 weight parts) and formic acid (1 weight part). The concentration of PCL was 9 wt%. The solution was stirred for 24 h at room temperature and then the electrospinning process was carried out using a Nanospider™ NSLAB 500 (ELMARCO). The PCL solution was electrospun with a 20 cm long wired electrode under a voltage of 55 kV. The distance between high voltage and ground electrodes was set to 100 mm. The high voltage electrode rotated at 5 rpm and the fabric collector at the grounded electrode moved at 12 mm/min. The resulting nanofibrous polymer foils were compact, flexible,

and homogenous with a thickness 30–40 μm. SEM images of the polymer nanofibers were acquired by Tescan LYRA3 in secondary emission mode at 10 kV acceleration voltage. To avoid charging of the sample surface, prior to the imaging, the samples were coated with a 10 nm thick gold film deposited by RF magnetron sputtering (Leica ACE 600).

2.2. Image Analysis Techniques

Image analysis was done using MATLAB. Two-phase approach has been designed to remove unwanted objects and compute diameter across various locations in the image. This approach employed segmentation methods based on the thresholding and deformable curve evolution model which are briefly explained in next sections.

2.2.1. Thresholding based segmentation

These methods can be categorized as global and local methods. A popular histogram-based Otsu algorithm assumes two classes pixels in an image, background and forground. It computes the threshold value separating two classes by minimizing between class variance. The adaptive methods are based on considering the local region around the pixel. We used the local thresholding methods by Sauvola [37] and Bradley [38]. Sauvola method calculates mean and variance at pixel positions whereas in the Bradley method threshold value is chosen for each pixel taking into account the integral image. These methods are chosen because of their known robustness under illumination changes. The Bradley method is faster than the Sauvola method, otherwise, segmentation performance is comparable. Both of these methods do suffer from the inability to account for inhomogeneity present across the boundary of nanotubes. The curve evaluation methods can better deal with inhomogeneity present in the data. These are explained in the next section.

2.2.2. Deformable models

The work [32] used implicit curves (level sets) to counter topological changes while curve evolution. Region-based model as a special case of Mumford Shah formulation [39] was inroduced by Chan-Vese [33]. This method does not require edge function for evolving. The inside and outside regions of the curve caused the deformation of the curve. Stopping of the curve takes place using minimization of the energy which lead it finally towards the boundary of the object. Let ϕ be the function describing level surface, u_0 the image, and u_{in} and u_{out} for the average intensities inside and outside of the respectively.

The evolution of the curve is encoded by Euler-Lagrange equation corresponding to the Mumford Shah functional:

$$\frac{\partial \phi}{\partial t} = \delta\phi \left(\mu \operatorname{div} \frac{\nabla \phi}{|\nabla \phi|} - \lambda_1 (u_0(x,\, y) - u_{in}(x,\, y)) \; + \; \lambda_2 (u_0(x,\, y) - u_{out}(x,\, y)) \right) \tag{1}$$

where, $\delta\phi$ is smoothened analog of the Dirac function related to ϕ.

Region-based methods are better in segmenting objects with uniformity but lead to inaccuracy for inhomogeneous cases. Brox et al [40] included local statistics into the variational framework. Lankton et al proposed [34] to introduce localization of global energy functional given by Chan-Vase [33]. In this work we have utilized both. As shown in Fig. 1, a bounding ball mask $\mathcal{B}(x, y)$ is chosen with a fixed radius r along the perimeter of contour considering inside and ouside regions locally. The localized Energy formulation, leads to the Euler-Lagrange equation:

$$\frac{\partial \phi}{\partial t}(x) = \delta\phi(x) \int_{\Omega_y} \mathcal{B}(x, y) \cdot \nabla_{\phi(y)} F(I(y), \phi(y))\, dy \;\; + \;\; \lambda \delta\phi(x) \operatorname{div} \left(\frac{\nabla \phi(x)}{|\nabla \phi(x)|} \right) \tag{2}$$

where the force function F is

$$F_{CV} = \mathcal{H}\phi(y)(u_0(y) - u_{in})^2 + \; (1 - \mathcal{H}\phi(y))(u_0(y) - u_{out})^2,$$

$\mathcal{H}$ is the smoothened Heaviside function related to ϕ, I is the segmented image, and u_i and u_o are mean values of the data inside and outside of evolving curve. See [34] for theory and implementation[1] details.

3. Results and discussion

The challenges posed while computing the diameter of nanotubes in the TEM images were following: the presence of supporting carbon holey membrane, overlapping tubes, catalytic iron nanoparticles, unfocused blurry tubes. Another obstacle observed was non-uniformity in illumination due to scattering of electrons on the irregular surface in high magnification images as shown in Fig. 3a. Previous work [13] used intensity profile across nanotubes which obeys Lambert's law to evaluate the diameter . However, the aforementioned issues cause loss of intensity information around the nanotubes boundary, which makes this method redundant.

[1] https://www.mathworks.com/matlabcentral/profile/authors/1306225

Algorithm 1 Computation of average diameter of nanotube in the selected region

Input: Grayscale section $S(x, y)$ and its segmented image $Seg(x, y)$ of size nxn

Output: Averaged diameter, in the section (nm)

1: Extract the middle curve (1-pixel width) by symmetric erosion from $Seg(x, y)$ innerSkel(x, y) is the skeleton image, $iL =$ length of middle curve
2: Apply Laplacian $\triangle(g(x, y))$ to extract outerSkel(x, y) which contains the outer boundary of the nanotube.
3: $sum = 0, num = 0$, $h = \frac{1}{8}n$
4: Loop1 $i = 1$ to $iL - h$
5: Set $xi = i$ to $i + h$ and $yj = j$ to $j + h$
6: Loop2 $k = 1$ to length(xi)
7: $Diameter =$ sweepNormal(xk, yk). This function is detailed in Algorithm 2.
8: $sum = sum + Diameter$, $num = num + 1$
9: end Loop2
10: end Loop1
11: Average diameter, $D = \dfrac{sum}{num} \times factor$ here, $factor = \dfrac{pixels}{nm}$

Algorithm 2 sweepNormal (xk,yk): To compute diameter (D) at individual points on the middle curve

Input: The coordinate of the middle curve (xk, yk), the set of coordinates of the normal obtained at (xk,yk) i.e (xN, yN), outerSkel is the image with boundary skeleton

Output: Diameter D

1: Loop1 $ix = xk$ to n
2: $it2 = xk - ix + 1$, This is the parameter on the normal line segment $it2 \in [0, 1]$
3: if outerSkel $(xN(it2), yN(it2)) \neq 0$, check if the normal hits the boundary
4: $t2 = it2$
5: end Loop1
6: Loop2 $ix = 1$ to xk
7: $it1 = xk - ix + 1$, This is the parameter for the normal line segment $it1 \in [0, 1]$
8: if outerSkel $(xN(it1), yN(it1)) \neq 0$, check if the normal hits the boundary
9: $t1 = it1$
10: end Loop2
11: $D = \sqrt{(xN(t2) - xN(t1))^2 + (yN(t2) - yN(t1))^2}$

The steps for two-phase method are shown in Fig. 2. In the first phase of approach goal is to obtain a region around approximate linear sections of the tubes across the whole image. The location of centroids of these sections are then computed. The square region around these centroids is considered in the second phase Fig. 3g. In first phase, adaptive thresholding is used for its ability to segment thinner nanotubes which Otsu and Sauvola failed to do. These methods merge the finer tubes with the background and hence omit the number of processed tubes in the second phase. In the first phase, segmentation and morphological operations can cause erroneous removal/addition of pixels which is in turn corrected in the second phase. Centroids of the thinned sections of tubes are evaluated. Rectangular regions centered around these centroids are chosen for further processing in the second phase. The size of the chosen region affects the linearity of extracted sections, in our case its set to 260x260 pixels experimentally. In the first phase, extraction of square regions comprising sections of tubes is of a prime concern than accuracy of segmentation, which is achieved in the second phase. In principle, the global active contour (G-AC) assumes the image consists of two uniform regions. So it merges other smaller insignificant regions, Fig. 4 shows this effect in comparison to other local and global threshold based methods. This property proved to be useful for extraction of only one object in the region of interest in the first step Fig. 7. It improves the computing of centroid closer to the correct location. Another observation to notice is inhomogeneity in intensities around boundaries, visible for such regions in Fig. 5a-c.

In the second phase, localized active contour (L-AC) method is utilized for achieving accuracy. Sensitivity of the localized method concerning local intensity variations cause extraction of more than one object in a square window, which could affect the evaluated location of the centroid. Therefore, location of the centroid is computed in the previous step using global curve evolution.

One disadvantage of the localized curve evolution method is the number of iterations as it considers neighboring regions across (red circles in Fig. 4) the whole evolving curve. To counter this problem, the dilated binarized output of the global method is chosen as an initial mask. It reduced the number of iterations from 2000 to 700 for all regions. G-AC and threshold-based segmentation methods tend to produce an eroded image, visible in Fig. 4 and 5. So, the output is dilated first to accommodate neigboring region around boundaries as depicted in Fig. 6. The circular structure has radius of 4 pixels in our experiments. Fig. 5 shows some of the difficult cases. In these cases local curve evolution method is promising. By varying the size of the structuring element in the dilation of the skeleton in the fourth step in flow chart, the number of square regions

and their locations can be tuned.

We applied the same approach for SEM image of PCL nanofibers as shown in Fig. 8. These images have uniformity in intensities around the fibers. So, global curve evolution is sufficient to produce correct segmentation. Nanofibers are solid filled structures whereas nanotubes are hollow structures. Also the nanofibers have a larger diameter than CNTs, thus can be imaged by SEM and it brings advantage of not seeing the internal structure. Thus nanofibers have more homogeneous intensities of pixels which results in easy and precise segmentation. In phase 1, the image regions are captured having no overlaps and relatively clear background. This step can be achieved automatically as described in flow chart for further processing. The image morphology operation, so involved, require tuning of parameters like structure elements for erosion/dilation/skeleton extraction. Once set these parameters can be used for a wider range of image classes. This step can be replaced with efficient semi-automatic method for avoiding tuning of the parameters without compromising overall processing time for an image. The regions can be chosen user interactively. It is worth to notice that the possible presence of nanotubes/fibers with large varying widths whereas size for the picked regions is square and fixed. User intervention is helpful in such cases. In phase 2, segmentation of nanotube/fiber from the background is achieved using both G-AC and L-AC methods. The efficiency of this step is crucial in final computation of the diameter by Algorithm 1 and 2. The size of the extracted nanotube should not be affected while segmentation. Algorithm 1 require the grayscale and segmented image of the region under consideration. The steps mentioned in algorithm 1 evaluates the mid-curve (shown as red in Fig. 9) and outer boundaries. The subroutine, algorithm 2, computes the intersecting coordinates of the normal (in green) at the mid-curve position with outer boundaries(in black). Finally, the line joining these points evaluates the diameter. Fig. 10a shows a comparison of computed diameters with manual (the ground truth using Gwyddion), L-AC and G-AC methods. The computed diameters with L-AC (black curve) is closer to the ground truth than G-AC (in blue). In the regions with higher variance, G-AC method fails considerably. The reason for this behavior lies in the inability of the method to account for inhomogeneities in intensities. Fig. 10b shows the comparison of segmentation efficiency of the two methods with Dice coefficients. L-AC method is efficient for wide range of regions. The segmentation step is crucial and its result should be closer to human perception [41]. The ground truth required for evaluating Dice coefficients is obtained by manually extracting nanotubes from the background using a free-hand image annotation tool in MATLAB.

In our experiments, we have used G-AC and L-AC methods for segmentation. The popular Otsu method in principle, is similar to G-AC, both are based upon an inter-class variation of intensities whereas L-AC is known to incorporate subtle intensity variations, thereby produce segmentation closer to the ground truth [34]. We created a bank of 50 images capturing regions with varying background intensities and having linear/curved nanotubes. Table 1 shows results from six such arbitrary regions. Diameter is computed using Gwyddion software manually which serves as the ground truth [42]. The relative errors of diameter computation with the L-AC method are smaller than G-AC. In order to compare the efficiency of segmentation Dice coefficient is evaluated. The values indicate the performance of L-AC is better for all kinds of regions. Fig. 9 depicts the result of inter-mediatory steps. The diameters are computed along with all locations of mid-curve (in red). The Fig. 9b, shows a slight curvature of the nanotube. The averaged value of these diameters is robust under repetitions. The SEM images have homogenous distribution of intensities, therefore the results are not shown exclusively because of similar outputs under the two methods.

4. Conclusion

In the present work, ability of curve evolution method over traditional threshold based methods is detailed for computing nanomaterial diameter. PCL nanofiber images have uniform intensities and the global curve method is sufficient for segmentation. Two phase approach is effective in extracting linear and curved nanotubes and thereby compute the diameter of carbon nanotubes even in difficult of cases, which otherwise is not achievable considering intensity profile alone. However, the regions containing overlapping tubes remain indistinguishable and currently have to be excluded by the user interactively. The local region diameter in L-AC method can be tuned to deal with variations in intensities across the boundary of tubes. Experimentally it is observed that the lower values (<7 pixels) can account for higher variations. The objective analysis suggests that for segmentation L-AC method is efficient irrespective of intensity variation in the region of interest. The algorithms presented here are able to compute diameter for wide range of tubular sections independent of variation in diameter across the tubes and their curvature. Apart from this, another direction worth considering as future work is to reduce the number of iterations in the localized curve evolution method.

Acknowledgement

This research was carried out under the project CEITEC 2020 (LQ1601) with financial support from the Ministry of Education, Youth and Sports of the Czech Republic (MEYS CR) under the National Sustainability Programme II. CzechNanoLab project LM2018110 funded by MEYS CR is gratefully acknowledged for the financial support of the experiments at CEITEC Nano Research Infrastructure. The authors are thankful to Jan Michalička for acquiring TEM images and Eva Dvořáková for SEM images.

References

[1] MS Dresselhaus, G Dresselhaus, Jean-Christophe Charlier, and E Hernandez. Electronic, thermal and mechanical properties of carbon nanotubes. *Philosophical Transactions of the Royal Society of London. Series A: Mathematical, Physical and Engineering Sciences*, 362(1823):2065–2098, 2004.

[2] Tom Grace, LePing Yu, Christopher Gibson, Daniel Tune, Huda Alturaif, Zeid Al Othman, and Joseph Shapter. Investigating the effect of carbon nanotube diameter and wall number in carbon nanotube/silicon heterojunction solar cells. *Nanomaterials*, 6(3):52, 2016.

[3] B Arash and Q Wang. Detection of gas atoms with carbon nanotubes. *Scientific reports*, 3:1782, 2013.

[4] Haifeng Liu, Xili Ding, Gang Zhou, Ping Li, Xing Wei, and Yubo Fan. Electrospinning of nanofibers for tissue engineering applications. *Journal of Nanomaterials*, 2013:3, 2013.

[5] Anton Manakhov, Elizaveta S Permyakova, Sergey Ershov, Alexander Sheveyko, Andrey Kovalskii, Josef Polčák, Irina Y Zhitnyak, Natalia A Gloushankova, Lenka Zajíčková, and Dmitry V Shtansky. Bioactive ticapcon-coated pcl nanofibers as a promising material for bone tissue engineering. *Applied Surface Science*, 479:796–802, 2019.

[6] Špela Zupančič, Liis Preem, Julijana Kristl, Marta Putrinš, Tanel Tenson, Petra Kocbek, and Karin Kogermann. Impact of pcl nanofiber mat structural properties on hydrophilic drug release and antibacterial activity on periodontal pathogens. *European Journal of Pharmaceutical Sciences*, 122:347–358, 2018.

[7] Dan-qing Liu, Zhi-qiang Cheng, Qing-jie Feng, He-jie Li, Shu-feng Ye, and Bo Teng. Polycaprolactone nanofibres loaded with 20 (s)-protopanaxadiol for in vitro and in vivo anti-tumour activity study. *Royal Society open science*, 5(5):180137, 2018.

[8] Morshed Khandaker, Shahram Riahinezhad, Harsha Jamadagni, Tracy Morris, Alexis Coles, and Melville Vaughan. Use of polycaprolactone electrospun nanofibers as a coating for poly (methyl methacrylate) bone cement. *Nanomaterials*, 7(7):175, 2017.

[9] Mohammad Ziabari, Vahid Mottaghitalab, Scott T McGovern, and AK Haghi. A new image analysis based method for measuring electrospun nanofiber diameter. *Nanoscale Research Letters*, 2(12):597, 2007.

[10] L Ghasemi-Mobarakeh, D Semnani, and M Morshed. A novel method for porosity measurement of various surface layers of nanofibers mat using image analysis for tissue engineering applications. *Journal of applied polymer science*, 106(4):2536–2542, 2007.

[11] K Oshida, M Murata, K Fujiwara, T Itaya, T Yanagisawa, K Kimura, T Nakazawa, YA Kim, M Endo, B-H Kim, et al. Structural analysis of nano structured carbon by transmission electron microscopy and image processing. *Applied Surface Science*, 275:409–412, 2013.

[12] William D Pyrz and Douglas J Buttrey. Particle size determination using tem: a discussion of image acquisition and analysis for the novice microscopist. *Langmuir*, 24(20):11350–11360, 2008.

[13] Cédric Gommes, Silvia Blacher, Karine Masenelli-Varlot, Ch Bossuot, Edward McRae, Antonio Fonseca, J-B Nagy, and J-P Pirard. Image analysis characterization of multi-walled carbon nanotubes. *Carbon*, 41(13):2561–2572, 2003.

[14] Yoichiro Iwasaki, Toshiyuki Nakamiya, Ryosuke Kozai, Fumiaki Mitsugi, and Toshihiko Ikegami. An image analysis algorithm to measure the diameters of carbon nanotubes. *Przeglad Elektrotechniczny*, 87:25–29, 01 2011.

[15] Dawid Saladra and Magdalena Kopernik. Qualitative and quantitative interpretation of sem image using digital image processing. *Journal of microscopy*, 264(1):102–124, 2016.

[16] M Salzer, Torben Prill, A Spettl, D Jeulin, K Schladitz, and V Schmidt. Quantitative comparison of segmentation algorithms for fib-sem images of porous media. *Journal of microscopy*, 257(1):23–30, 2015.

[17] Y Sharma, AB Phillion, and DM Martinez. Automated segmentation of wood fibres in micro-ct images of paper. *Journal of microscopy*, 260(3):400–410, 2015.

[18] Jun Qiu and F-F LI. Quantitative morphological analysis of curvilinear network for microscopic image based on individual fibre segmentation (ifs). *Journal of microscopy*, 256(3):153–165, 2014.

[19] Dongjae Kim, Jungkyu Choi, and Jaewook Nam. Entropy-assisted image segmentation for nano-and micro-sized networks. *Journal of microscopy*, 262(3):274–294, 2016.

[20] DJ Groom, K Yu, S Rasouli, J Polarinakis, AC Bovik, and PJ Ferreira. Automatic segmentation of inorganic nanoparticles in bf tem micrographs. *Ultramicroscopy*, 194:25–34, 2018.

[21] Benjamin R Bunes, Palma E Catravas, and Michael E Hagerman. Image processing algorithm for analyzing chirality in carbon nanotubes. In *2008 8th IEEE Conference on Nanotechnology*, pages 424–427. IEEE, 2008.

[22] Xiao-ning Liang and Wei Li. Fractal and digital image processing to determine the degree of dispersion of carbon nanotubes. *Journal of Nanoparticle Research*, 18(5):136, 2016.

[23] Daniel S Raimundo, Priscila B Calíope, Danilo R Huanca, and Walter J Salcedo. Anodic porous alumina structural characteristics study based on sem image processing and analysis. *Microelectronics Journal*, 40(4-5):844–847, 2009.

[24] Udomchok Phromsuwan, Yaowarat Sirisathitkul, Chitnarong Sirisathitkul, Paisarn Muneesawang, and Bunyarit Uyyanonvara. Quantitative analysis of x-ray lithographic pores by sem image processing. *Mapan*, 28(4):327–333, 2013.

[25] Josef Kittler and John Illingworth. Minimum error thresholding. *Pattern recognition*, 19(1):41–47, 1986.

[26] T Pun. Entropic thresholding, a new approach. *Computer Graphics and Image Processing*, 16(3):210 – 239, 1981.

[27] Ahmed S Abutaleb. Automatic thresholding of gray-level pictures using two-dimensional entropy. *Computer vision, graphics, and image processing*, 47(1):22–32, 1989.

[28] Liang-Kai Huang and Mao-Jiun J Wang. Image thresholding by minimizing the measures of fuzziness. *Pattern recognition*, 28(1):41–51, 1995.

[29] Shimon D Yanowitz and Alfred M Bruckstein. A new method for image segmentation. *Computer Vision, Graphics, and Image Processing*, 46(1):82–95, 1989.

[30] Khang Siang Tan and Nor Ashidi Mat Isa. Color image segmentation using histogram thresholding–fuzzy c-means hybrid approach. *Pattern Recognition*, 44(1):1–15, 2011.

[31] Nobuyuki Otsu. A Threshold Selection Method from Gray-level Histograms. *IEEE Transactions on Systems, Man and Cybernetics*, 9(1):62–66, 1979.

[32] Stanley Osher and James A Sethian. Fronts propagating with curvature-dependent speed: algorithms based on hamilton-jacobi formulations. *Journal of computational physics*, 79(1):12–49, 1988.

[33] Tony F Chan and Luminita A Vese. Active contours without edges. *IEEE Transactions on image processing*, 10(2):266–277, 2001.

[34] Shawn Lankton and Allen Tannenbaum. Localizing region-based active contours. *IEEE transactions on image processing*, 17(11):2029–2039, 2008.

[35] P Kaushik, M Eliáš, J Michalička, D Hegemann, Z Pytlíček, D Nečas, and L Zajíčková. Atomic layer deposition of titanium dioxide on multi-walled carbon nanotubes for ammonia gas sensing. *Surface and Coatings Technology*, 370:235–243, 2019.

[36] Anton Manakhov, Eva Kedroňová, Jiřina Medalová, Petra Černochová, Adam Obrusnik, Miroslav Michlíček, Dmitry V Shtansky, and Lenka Zajíčková. Carboxyl-anhydride and amine plasma coating of pcl nanofibers to improve their bioactivity. *Materials & Design*, 132:257–265, 2017.

[37] Jaakko Sauvola and Matti Pietikäinen. Adaptive document image binarization. *Pattern recognition*, 33(2):225–236, 2000.

[38] Derek Bradley and Gerhard Roth. Adaptive thresholding using the integral image. *Journal of graphics tools*, 12(2):13–21, 2007.

[39] David Mumford and Jayant Shah. Optimal approximations by piecewise smooth functions and associated variational problems. *Communications on pure and applied mathematics*, 42(5):577–685, 1989.

[40] Thomas Brox and Daniel Cremers. On the statistical interpretation of the piecewise smooth mumford-shah functional. In *International Conference on Scale Space and Variational Methods in Computer Vision*, pages 203–213. Springer, 2007.

[41] Peter Bajcsy, Mylene Simon, SJ Florczyk, Carl G Simon Jr, Derek Juba, and MC Brady. A method for the evaluation of thousands of automated 3d stem cell segmentations. *Journal of microscopy*, 260(3):363–376, 2015.

[42] David Nečas and Petr Klapetek. Gwyddion: an open-source software for spm data analysis. *Open Physics*, 10(1):181–188, 2012.

List of figure captions

Fig. 1 The local contours across the boundary of evolving curve.

Fig. 2 Flow Chart: Steps involving the two-phase approach.

Fig. 3 Phase 1 steps in figures a) to g) and h) shows one of the selected square region from g) required in Phase 2 to compute the diameter.

Fig. 4 a) Section of nanotube with blurred tube in the neighbourhood and non uniformity of intensities is visible, b) Otsu threshold, c) Sauvola method with 15x15 window, d) Global active contour, e) Maximum entropy threshold, f) Localized active contour (radius=5), g) Bradley method and h) Comparison of global and local active contour methods in red and green colors repectively.

Fig. 5 Examples of sections with results showing comparison of global active contour (red circle) and localized active contour methods (green circle, circular region with radius=5).

Fig. 6 Left figure: The green and red circles depict the result of localized active contour and global active contour method respectively (the respective diameters are the size of nanotubes). Right figure: Shows intensity profile along the diameter of the section of nanotube, inconsistency in intensities is visible.

Fig. 7 Initial mask for localized curve evolution, from left to right: a) Grayscale image b) Global curve segmented image c) Dilated image with local regions (radius=4) indicated in red circles d) Final outcome.

Fig. 8 SEM images a) PCL nanofiber image b) A section of nanofiber (encircled red in a), performance of both curve evolution methods is similar.

Table 1 The computed diameters in phase 2, errors due to global and local curve evolution methods with Gwyddion and comparison of Dice coefficients (DC)

Region number	**Std. Dev. (intensities)**	**Diameter (nm)**			**Diameter error**		**DC**	
		L-AC	**G-AC**	**Gwyiddion**	**L-AC**	**G-AC**	**L-AC**	**G-AC**
1	24.41	26.98	25.02	26.2	0.03	0.05	0.99	0.96
14	20.55	23.92	20.14	24	0	0.16	0.99	0.89
15	20.43	24.66	13.37	26.2	0.06	0.49	0.99	0.82
22	26.22	19.95	18.25	20	0	0.09	0.99	0.95
28	25.48	20.58	17.29	20.7	0.71	0.19	0.98	0.95
30	30.81	21.99	21.22	23.5	0.74	0.04	0.99	0.99

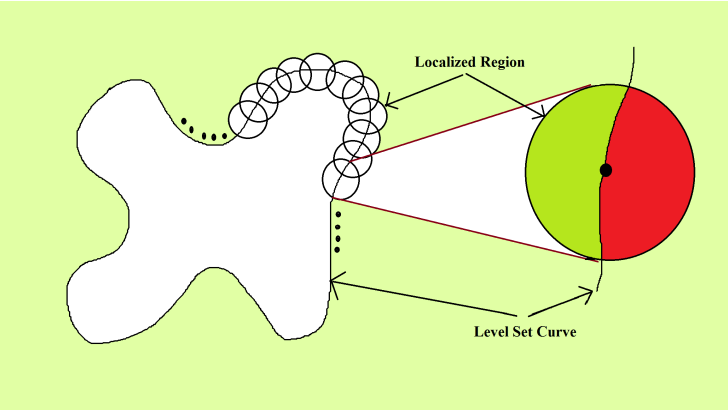

Fig. 1. The local contours across the boundary of evolving curve.

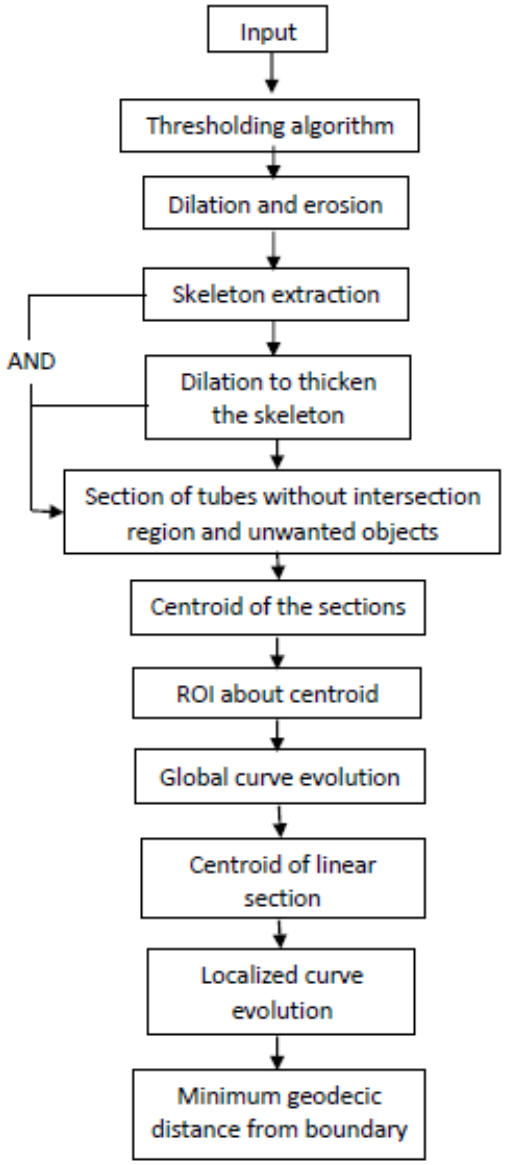

Fig. 2. Flow Chart: Steps involving the two-phase approach.

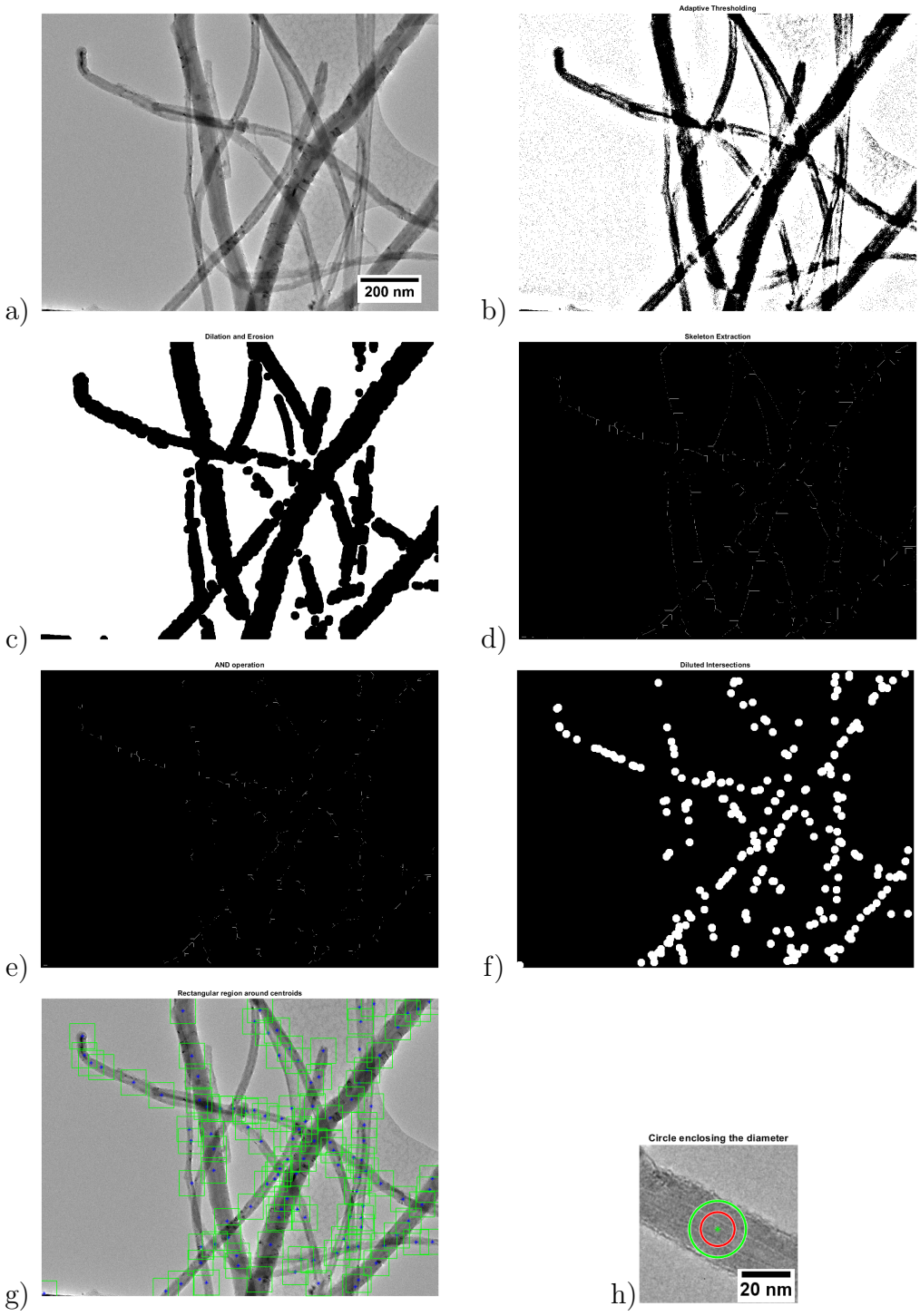

Fig. 3. Phase 1 steps in figures a) to g) and h) shows one of the selected square region from g) required in Phase 2 to compute the diameter.

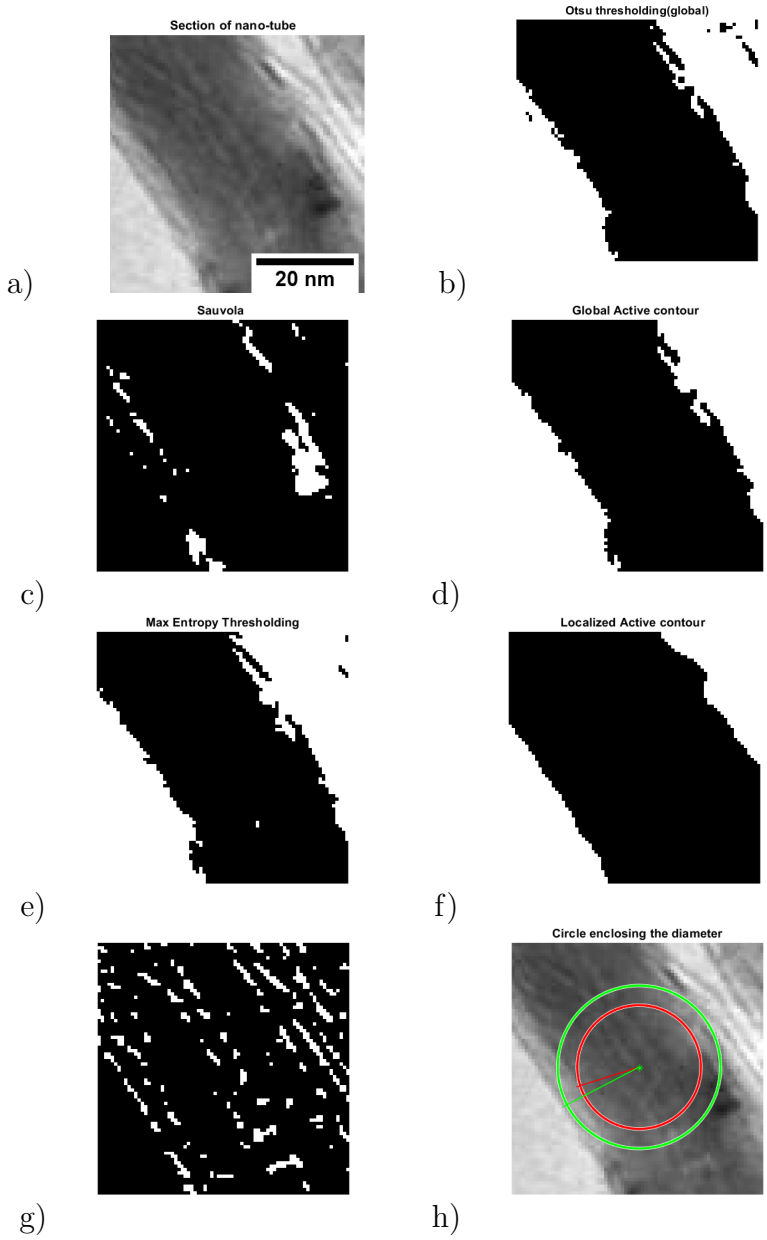

Fig. 4. a) Section of nanotube with blurred tube in the neighbourhood and non uniformity of intensities is visible, b) Otsu threshold, c) Sauvola method with 15x15 window, d) Global active contour, e) Maximum entropy threshold, f) Localized active contour (radius=5), g) Bradley method and h) Comparison of global and local active contour methods in red and green colors repectively.

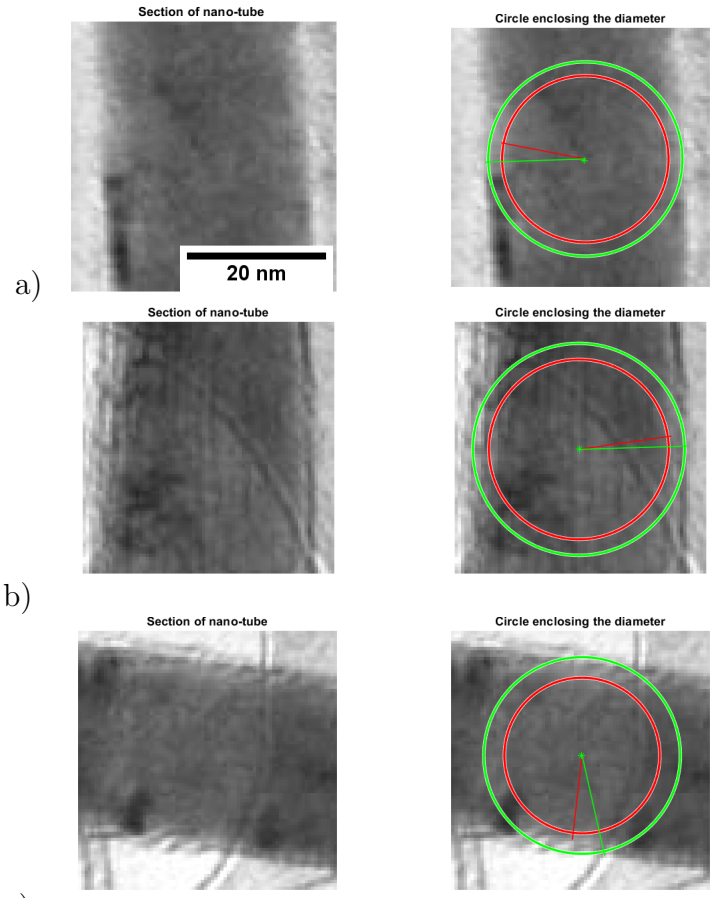

Fig. 5. Examples of sections with results showing comparison of global active contour (red circle) and localized active contour methods (green circle, circular region with radius=5).

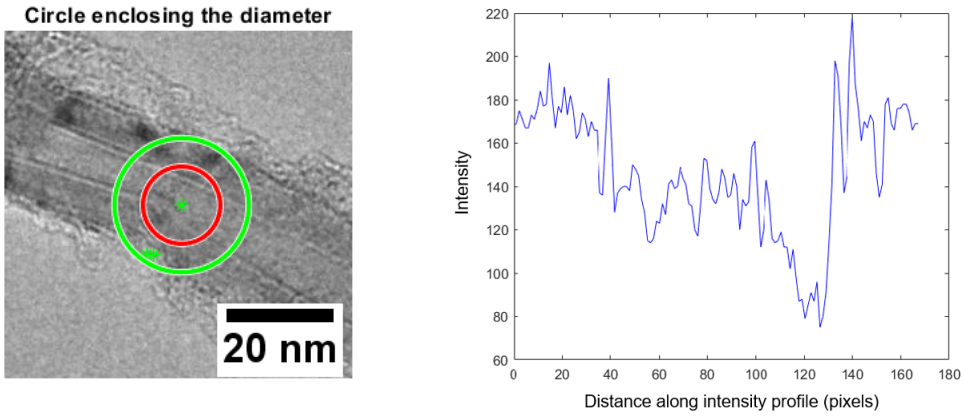

Fig. 6. Left figure: The green and red circles depict the result of localized active contour and global active contour method respectively (the respective diameters are the size of nanotubes). **Right figure:** Shows intensity profile along the diameter of the section of nanotube, inconsistency in intensities is visible.

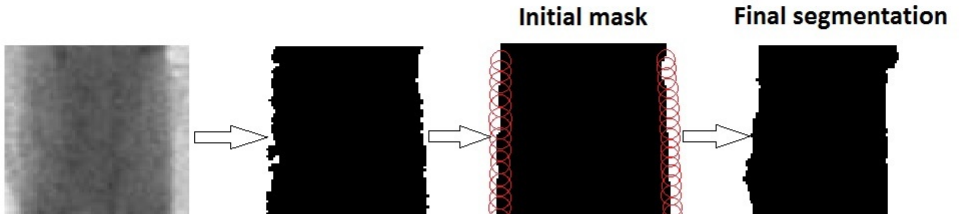

Fig. 7. Initial mask for localized curve evolution, from left to right: a) Grayscale image b) Global curve segmented image c) Dilated image with local regions (radius=4) indicated in red circles d) Final outcome.

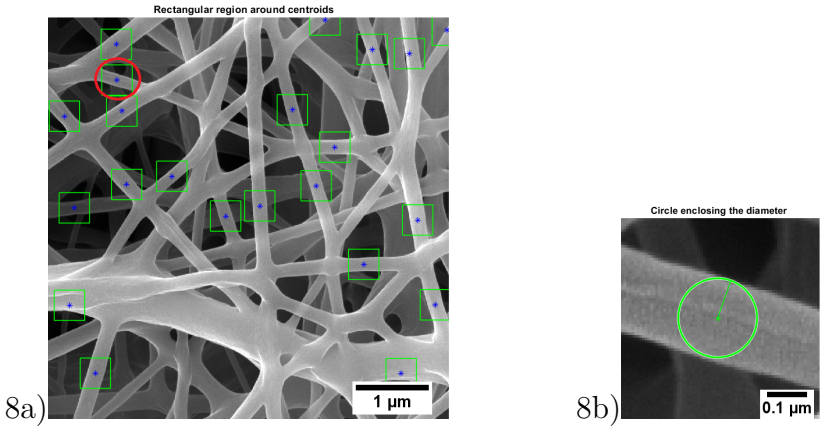

8a) 8b)

Fig. 8. SEM images a) PCL nanofiber image b) A section of nanofiber (encircled red in a), performance of both curve evolution methods is similar.

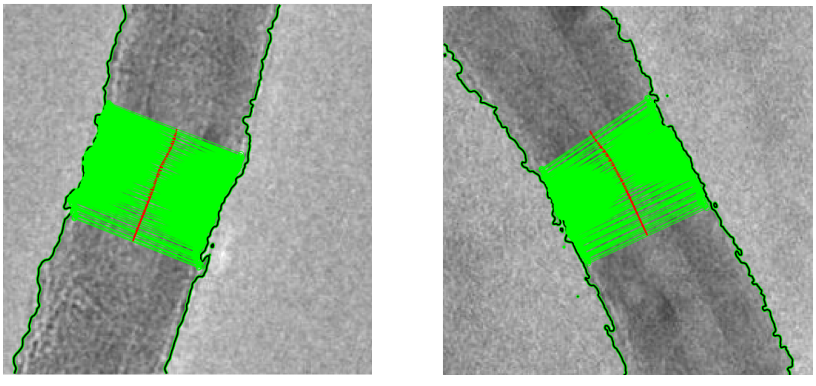

(a) (b)

Fig. 9. Computation of diameter in phase 2: a) linear CNTs and b) slightly curved CNTs

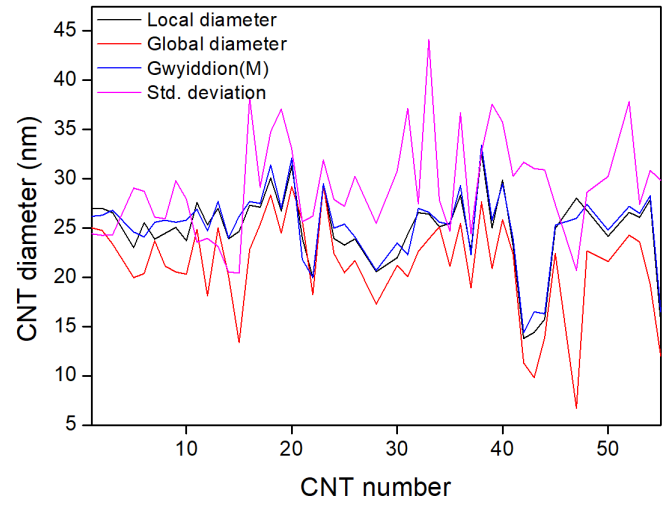

(a)

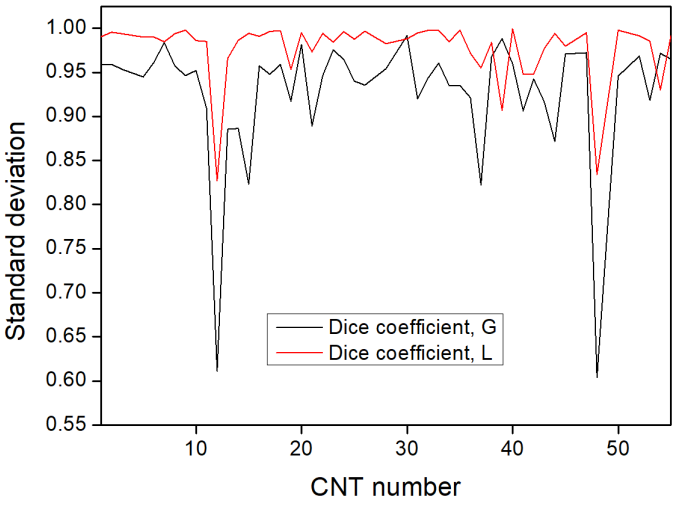

(b)

Fig. 10. a) Comparison of diameter by G-AC, L-AC and manual method (Gwyddion) b) comparative efficiency of segmentation